Neuron
Article

Dynamic Microtubules Regulate Dendritic Spine Morphology and Synaptic Plasticity

Jacek Jaworski,[1,4,7] Lukas C. Kapitein,[1,7] Susana Montenegro Gouveia,[2,7] Bjorn R. Dortland,[1,7] Phebe S. Wulf,[1] Ilya Grigoriev,[2] Paola Camera,[6] Samantha A. Spangler,[1] Paola Di Stefano,[6] Jeroen Demmers,[3] Harm Krugers,[5] Paola Defilippi,[6] Anna Akhmanova,[2] and Casper C. Hoogenraad[1,*]
[1]Department of Neuroscience
[2]Department of Cell Biology and Genetics
[3]Proteomics Center
Erasmus Medical Center, 3015 GE, Rotterdam, The Netherlands
[4]International Institute of Molecular and Cell Biology, Warsaw, Poland
[5]Swammerdam Institute for Life Sciences, University of Amsterdam, The Netherlands
[6]Molecular Biotechnology Center, University of Torino, Italy
[7]These authors contributed equally to this work
*Correspondence: c.hoogenraad@erasmusmc.nl
DOI 10.1016/j.neuron.2008.11.013

SUMMARY

Dendritic spines are the major sites of excitatory synaptic input, and their morphological changes have been linked to learning and memory processes. Here, we report that growing microtubule plus ends decorated by the microtubule tip-tracking protein EB3 enter spines and can modulate spine morphology. We describe p140Cap/SNIP, a regulator of Src tyrosine kinase, as an EB3 interacting partner that is predominately localized to spines and enriched in the postsynaptic density. Inhibition of microtubule dynamics, or knockdown of either EB3 or p140Cap, modulates spine shape via regulation of the actin cytoskeleton. Fluorescence recovery after photobleaching revealed that EB3-binding is required for p140Cap accumulation within spines. In addition, we found that p140Cap interacts with Src substrate and F-actin-binding protein cortactin. We propose that EB3-labeled growing microtubule ends regulate the localization of p140Cap, control cortactin function, and modulate actin dynamics within dendritic spines, thus linking dynamic microtubules to spine changes and synaptic plasticity.

INTRODUCTION

Dendritic spines are membrane protrusions that are the major sites of glutamatergic presynaptic input in the mammalian central nervous system. Although small in size (up to a few microns in length), spines are motile and remarkably diverse in size and shape, ranging from long, thin filopodia-like protrusions to mushroom-shaped spines (Harris and Kater, 1994; Hering and Sheng, 2001). Nearly all dendritic spines contain a postsynaptic density (PSD), a complex matrix of postsynaptic receptors, signaling molecules and cytoskeletal proteins involved in postsynaptic signaling and plasticity (Kennedy et al., 2005; Sheng and Hoogenraad, 2007). The strong correlation between the size of the spine and the strength of the synapse makes spine remodeling an attractive structural mechanism underlying learning and memory (Kasai et al., 2003; Lamprecht and LeDoux, 2004; Yuste and Bonhoeffer, 2001). In addition, several human mental retardation syndromes have been linked to altered spine morphology (Hering and Sheng, 2001; Kaufmann and Moser, 2000; Newey et al., 2005).

Biochemical events that regulate dendritic spine remodeling are poorly understood. It is generally believed that changes in spine morphology are based on rearrangements of the actin cytoskeleton (Ethell and Pasquale, 2005; Matus, 2000; Tada and Sheng, 2006). Within spines, actin is present as a soluble pool of monomeric G-actin and as polymerized F-actin filaments that confer the characteristic spine shape. Multiple signaling pathways, particularly those involving small GTPases of the Rho and Ras family, control actin organization (Ethell and Pasquale, 2005; Newey et al., 2005; Tada and Sheng, 2006). Recently, members of the Src family of non-receptor tyrosine kinases were also found in dendritic spines and implicated in spine reorganization, most likely through controlling actin polymerization (Morita et al., 2006; Webb et al., 2007). However, it remains unclear how different signal transduction pathways converging on the actin-based processes within spines are coordinated.

There is strong evidence that in nonneuronal cells the microtubule (MT) cytoskeleton serves as a primary spatial regulator of cell shape. MTs are highly dynamic and can interact with actin in areas of cellular growth or reorganization during cell division, polarization, and migration (Rodriguez et al., 2003; Siegrist and Doe, 2007). In developing neurons, the actin and MT cytoskeleton also act together to guide and support the growth and differentiation of axons and dendrites (Dent and Gertler, 2003). In contrast to these well-studied examples of MT-actin cooperativity, it is widely accepted that in dendrites of mature neurons the two cytoskeletal domains are spatially separated; while actin filaments are predominately concentrated in spines, stable MTs are confined to the dendritic shaft and do not branch off into spines (Matus, 2000). This view is based on ultrastructural and

fluorescent imaging studies showing that MTs and MT-associated protein 2 (MAP2) are absent from dendritic spines (Kaech et al., 2001; Landis and Reese, 1983). While this revealed that stable MTs, decorated with MAP2, are predominantly present as bundles in dendritic shafts, it is currently unknown whether dynamic MTs are involved in the regulation of dendritic spine morphology and synaptic plasticity.

Dynamic MTs can be distinguished from stable ones by a number of markers; in particular, growing MTs specifically accumulate a set of factors known as MT plus-end tracking proteins, or +TIPs at their ends (Akhmanova and Hoogenraad, 2005). +TIPs are thought to be important for cross-talk between dynamic MTs and actin (Basu and Chang, 2007; Rodriguez et al., 2003); moreover, they can be used as tools to visualize growing MT ends even within dense MT networks (Morrison et al., 2002; Stepanova et al., 2003). Among +TIPs, proteins of the EB family directly interact with the majority of other known plus-end binding proteins and have been implicated as key regulators of MT-associated signaling pathways (Jaworski et al., 2008; Lansbergen and Akhmanova, 2006).

Here, we use a large variety of biochemical, cell-biological, and quantitative/high-resolution microscopic approaches to determine the potential role of +TIPs in spine morphogenesis. We show that dynamic EB3 positive MT plus ends can enter dendritic spines, are required for controlling the levels of F-actin within the spines, and are essential for the maintenance of spine morphology and mature synapses. Furthermore, we found that p140Cap, a regulator of Src tyrosine kinase, associates with EB3 and F-actin binding protein cortactin. We propose a model in which EB3 regulates spine size by modulating the turnover of p140Cap in spines, thereby altering actin dynamics through the regulation of cortactin.

RESULTS

EB3 Expression Increases during Neuronal Maturation

Several +TIPs have been shown to localize to MT plus ends in developing neuronal cells (reviewed in Jaworski et al., 2008). However, very little is known about localization and function of +TIPs in mature neurons. To identify +TIPs abundant in hippocampal neurons at the time of spine maturation we probed western blots of homogenates of cultured hippocampal neurons for different +TIPs (Figure 1A and data not shown). Most +TIPs analyzed were already expressed at in vitro day 3 (DIV 3) and slightly increased during neuronal development. However, EB3 was undetectable in young neurons (<DIV 7) and began to elevate throughout development with the strongest expression in more mature neurons (>DIV 17) (Figure 1A). This is consistent with high levels of EB3 expression in vivo in the adult hippocampus and cerebral cortex compared to embryonic and postnatal stages (Figure 1B).

Next, we stained different stages of developing and mature hippocampal neurons (from DIV 3 to DIV 21) with antibodies against the three mammalian EB family members, EB1, EB2, and EB3. While anti-EB2 antibodies produced no clear pattern (data not shown), EB1, and EB3-specific staining appeared as dashes or comets, which have been shown to correspond to growing MT tips in numerous studies (Komarova et al., 2005; Stepanova et al., 2003). Interestingly, EB1 and EB3 displayed different developmental patterns: EB1-positive dashes were clearly visible in young hippocampal neurons at < DIV 7 but not in mature cells, whereas EB3 immunoreactivity was hard to detect in developing neurons but was highly prominent in mature neurons at > DIV17 (Figures 1C, 1D, 1F, S1A, S1B, and S1D). High levels of EB3 expression correlate with fully developed neurons with mushroom-headed spines positive for the postsynaptic marker PSD-95 (Figures S1C and S1E). The lack of changes in EB1 expression by immunoblot (Figure 1A) can be attributed to the abundance of EB1 in glial cells in both developing and mature neuronal cultures (Figure 1F).

The robust switch in EB family proteins during neuronal development is most likely regulated at the level of gene expression. To test whether reduced EB3 expression is able to induce EB1 levels in older neurons, we used DNA plasmid (pSuper)-based RNA interference to knock down endogenous EB3 (Komarova et al., 2005). Dissociated hippocampal neurons in culture at DIV13 were transfected with EB3-shRNA together with β-galactosidase (β-gal), to highlight shRNA expressing cells. Four days after transfection, the EB3-specific antibody showed ~90% reduction in staining intensity in neurons transfected with the EB3-shRNA construct (Figures 1E and 1G). EB1 staining was unchanged in neurons transfected with EB3-shRNA (Figures 1E and 1G), indicating that EB1 expression is not increased by reduction of EB3 levels. We conclude that EB3 proteins levels are steadily increased during neuronal development and its expression and abundance at MT tips peaks in mature neurons.

MT Plus Ends Labeled with Endogenous EB3 or EB3-GFP Enter Dendritic Spines

Next, we examined in detail the subcellular distribution of EB3 in mature dendrites. Cultured hippocampal neurons (> DIV 17) stained with EB3-specific antibodies showed characteristic comet-like MT plus-end patterns (Figure 2A). Similar to non-neuronal cells (Figure S2A) (Mimori-Kiyosue et al., 2000), blocking MT dynamics by the addition of 200 nM nocodazole completely abolished EB3-positive comets (Figures 2B and S2E; Stepanova et al., 2003). This effect was specific, since the MT network was still present, as indicated by MAP2 and tubulin costaining (Figures S2B and S2C); EB3 and tubulin expression was unchanged (Figure S2F) and polymerized MT levels measured by tubulin pre-extraction (He et al., 2002) were not significantly affected (Figures S2C and S2D). As expected (Mimori-Kiyosue et al., 2000; Stepanova et al., 2003), treatment with a low dose of taxol (200 nM) showed similar effects (Figures S2B–S2E). Taken together, these results suggest that in mature neurons endogenous EB3 specifically associates with the ends of growing MTs.

Although present in axons, EB3 staining was predominantly localized within the dendritic compartment, as revealed by the dendritic marker MAP2 (Figure 2A). However, to our surprise, EB3-labeled comets occasionally extended beyond the dendritic shaft (arrowheads in Figure 2A), overlapped with the synaptic marker Bassoon (arrowheads in Figure 2B) and localized within the dendritic spines visualized in β-gal filled neurons (Figure 2C). At DIV 17, we observed that a small fraction (on average 4%) of dendritic spines contained endogenous EB3

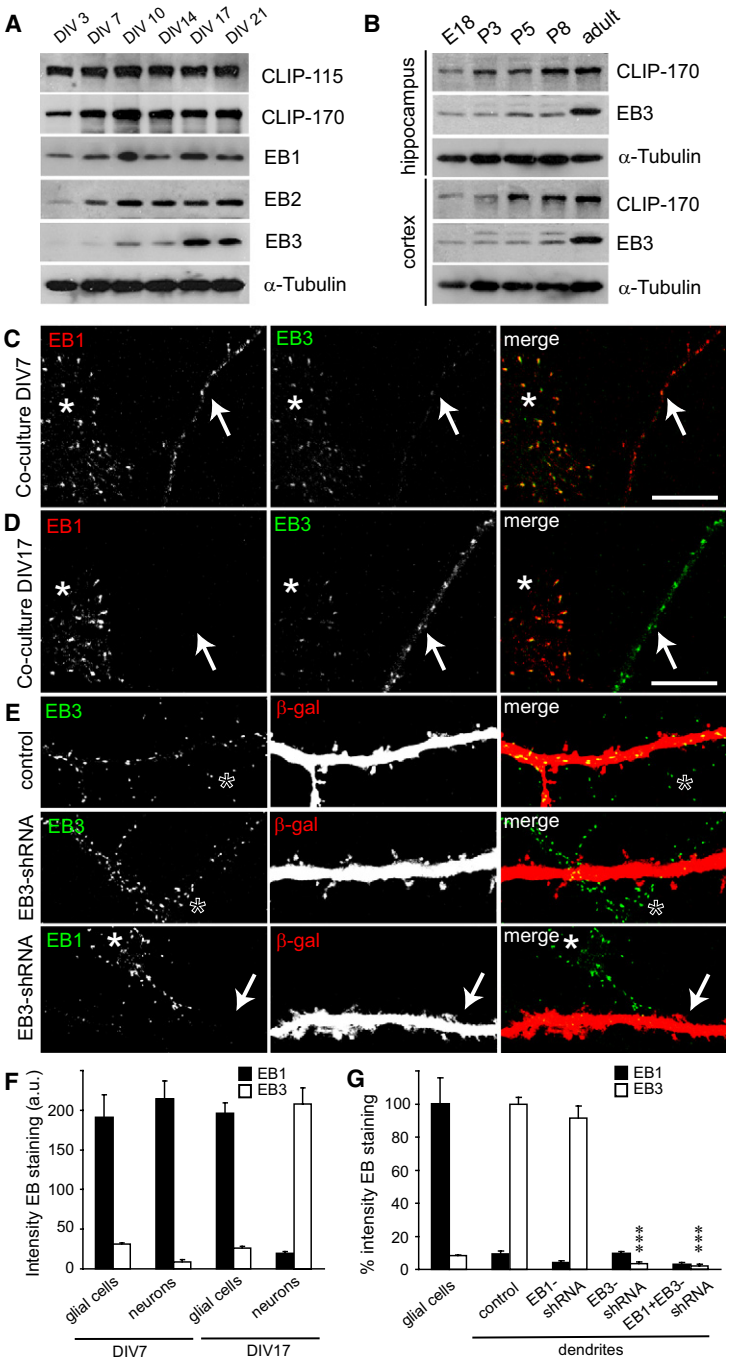

Figure 1. EB3 Expression Increases during Neuronal Development

(A) +TIP developmental expression patterns in cultured hippocampal neurons from DIV 3 to DIV 21 (20 μg of protein/lane).

(B) Patterns of developmental expression of CLIP-170 and EB3 in E18, P3, P5, P8, and 6-month-old (adult) rat hippocampus and cortex (20 μg of protein/lane).

(C and D) Representative images of rat hippocampal neurons at 7 DIV and 17 DIV double labeled with mouse anti-EB1 antibody (red) and rabbit anti-EB3 antibody (green). Only the merge is shown in color. Glial cells are indicated by a filled asterisk, and arrows point to neurons.

(E) Representative images of hippocampal neurons transfected at DIV 13 with control pSuper vector or EB3-shRNA and double labeled with anti-EB1 or anti-EB3 antibody (green) and for cotransfected β-gal (red). Nontransfected neurons are indicated by an open asterisk.

(F) Quantification of EB1 and EB3 immunostaining intensities (as arbitrary units) in dendrites of hippocampal neurons and glial cells in the same culture at DIV 7 and DIV 17.

(G) Quantification of EB1 and EB3 immunostaining intensities (mean ± SEM) in dendrites of hippocampal neurons transfected at DIV 13 for 4 days with control pSuper vector, EB1-shRNA, EB3-shRNA, or a combination of EB1-shRNA and EB3-shRNA. EB3 intensity in neurons is normalized to dendritic EB3 staining in pSuper control neurons. EB1 intensity in neurons is normalized to EB1 staining in glial cells. ***$p < 0.0005$.

staining. Among these, mushroom-shaped spines were slightly more frequent than thin filopodia; the few EB3-positive filopodia-like protrusions were typically long (>5 μm) and could represent newly forming dendritic arbors (data not shown). These data indicate that MT tips decorated with endogenous EB3 can enter dendritic spines.

To confirm this remarkable finding, we used the Semliki Forest virus (SFV) to deliver EB3-GFP to mature (DIV 21) hippocampal neurons in culture and analyzed its dynamics by live cell imaging. In cases when the expression level of EB3-GFP was low, we observed bidirectional displacements of EB3-GFP comets in hippocampal dendrites, whereas in axons the movements were unidirectional, reflecting different MT organization in axons and dendrites (Jaworski et al., 2008; Stepanova et al., 2003). The average velocity of EB3-GFP movement in mature hippocampal neurons was 0.12 ± 0.03 μm/s (mean ± SD; n > 500) and 1.8-fold lower than previously reported for young neurons (Stepanova et al., 2003). Although most EB3-GFP-positive comets moved along the dendritic shaft, a number of EB3-GFP dashes entered the spines and disappeared close to the head of the spine, most likely because of MT catastrophe (Figure 2E; Movie S1). EB3-GFP comets could target numerous spines on a single dendrite (Movie S2) or repeatedly enter the same spine (Figure 2F; Movie S3).

Overexpression of EB3 resulted in even distribution along the MT lattice (Komarova et al., 2005) and showed a significant increase of EB3-positive MTs pointing into the dendritic spines and colocalizing at their tips with synaptic markers (Figures 2D and 7F). Quantification revealed that EB3-positive MTs could be detected in ~30% of dendritic spines in EB3-GFP overexpressing neurons. Together these data indicate the presence of EB3-labeled MT tips in dendritic protrusions of mature neurons.

Dynamic MTs Affect Synaptic Plasticity and Spine Morphology in Hippocampal Slices

What is the function of dynamic MTs in mature neurons? To address this question, we utilized low concentrations of nocodazole to inhibit MT dynamics (Figure S2) (Mimori-Kiyosue et al.,

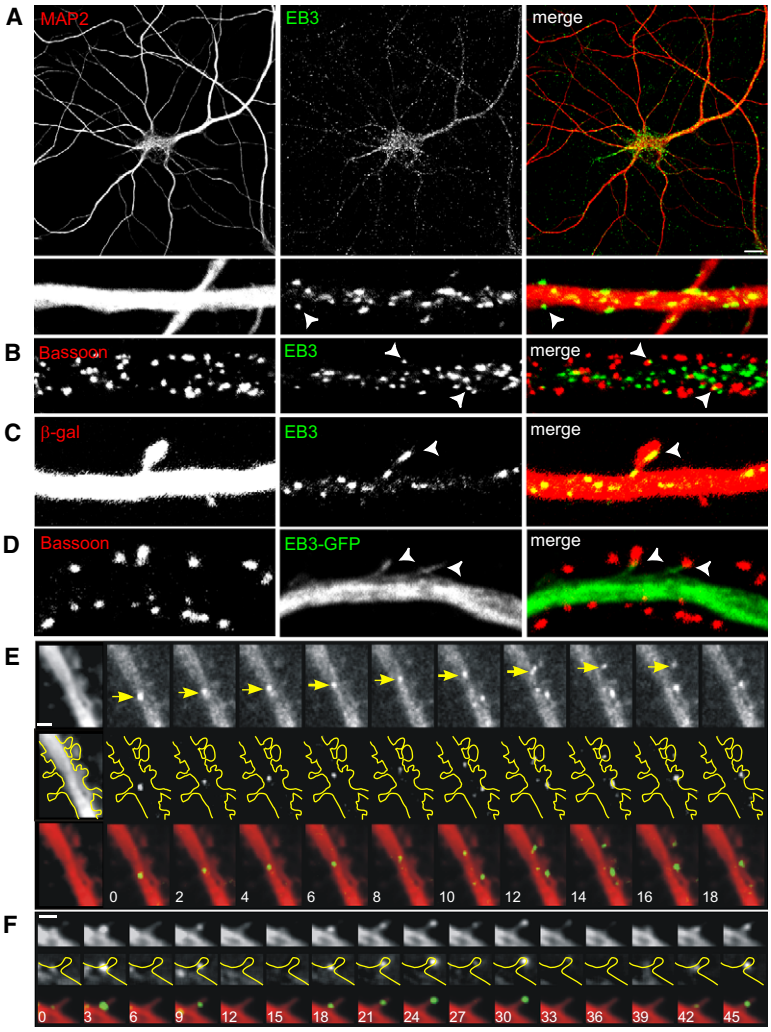

Figure 2. MT Plus-End-Bound EB3 Enters Dendritic Spines

(A) Representative images of rat hippocampal neurons (DIV 17) double labeled with rabbit anti-EB3 antibody (green) and mouse anti-MAP2 antibody (red). Only the merge is shown in color. Dendritic segments (lower panels) are enlarged to show the localization of EB3 and MAP2. Arrowheads indicate EB3 comets outside the dendritic shaft. Scale bar, 10 μm.

(B) Dendrites of hippocampal neurons labeled with rabbit anti-EB3 antibody (green) and mouse anti-Bassoon (red). Arrowheads indicate colocalization between EB3 and Bassoon.

(C) Hippocampal neurons transfected at DIV 13 with β-gal construct to visualize neuronal morphology and labeled with rabbit anti-EB3 antibody (green) and mouse anti-β-gal (red). Arrowheads indicate endogenous EB3 in dendritic spines.

(D) Hippocampal neurons transfected at DIV 13 with EB3-GFP and labeled with mouse anti-Bassoon (red). Arrowheads indicate colocalized EB3-GFP with Bassoon.

(E and F) Time-lapse recordings of EB3-GFP-infected neurons showing one (E) and multiple (F) EB3-GFP comets penetrating into spines. First image in all three rows shows neuron morphology obtained by averaging all frames from the time-lapse recording. Subsequent images show low-pass-filtered time series in row 1, low-pass-filtered time series with average of all frames subtracted and dendrite outline traced in yellow in row 2, and a merge of row 2 and the average of all frames in row 3. Scale bar is 1 μm, time in seconds.

2000; Vasquez et al., 1997) and abolish the binding of EB3 to MT ends in brain slices. We used organotypic slices of the hippocampus biolistically transfected with GFP to visualize neuronal morphology. CA1 neurons of hippocampal slice cultures treated for 4 hr with 200 nM nocodazole lost most of their mushroom-headed spines and instead displayed filopodia-like processes with reduced heads both on the apical and basal dendrites (Figure 3A). Next, dendritic protrusions were classified as filopodia-shaped protrusions and mushroom-shaped spines based on the ratio of spine head width to protrusion length (see Experimental Procedures). Nocodazole treatment decreased the number of mushroom-headed spines and increased the number of filopodia (Figure 3B), while the total number of dendritic protrusions was unaffected (Figure 3B). Nocodazole did not alter cell soma circumference, dendrite length, or dendrite width (Figure 3C and data not shown).

Since several studies have demonstrated a strong correlation between defects in synaptic plasticity and abnormalities in dendritic spine morphology (Yuste and Bonhoeffer, 2001), we next tested the effect of low doses of nocodazole on long-term potentiation in the Schaffer collateral-CA1 pathway in acute mouse hippocampal slices. High-frequency stimulation in the hippocampal CA1 area in control slices caused a transient and highly robust posttetanic rise in the slope of the field excitatory postsynaptic potentials (fEPSP) followed by a sustained increase in the synaptic response (Figure 3D). This stable synaptic potentiation was significantly suppressed in slices treated with 200 nM nocodazole (Figure 3D). Synaptic responses were depressed to almost baseline levels after 2 hr exposure to the drug (Figure 3D), suggesting a link between dynamic MTs and synaptic plasticity. Control experiments show no decline in fEPSP size 2 hr after nocodazole treatment. Although we cannot exclude that nocodazole treatment has an indirect effect on the synaptic response, it seems likely that the defects in synaptic plasticity in the absence of dynamic MTs are secondary to the disruption of spine/synaptic architecture.

EB3 Depletion Causes Spine Loss

To investigate the relationship between dynamic MTs and spines in more detail, we again switched to dissociated neuronal cultures. At DIV 17, control neurons exhibited mostly mushroom-shaped spines (Figure 4A). Treatment with low doses of nocodazole (200 nM, 4 hr) did not affect the total number of dendritic protrusions, but markedly reduced the number of spines and increased the number of filopodia, similar to the effects observed in slices. Loss of spines was already visible after 2 hr of nocodazole treatment but was not detectable within 30 min of incubation (data not shown), indicating that dynamic MTs influence the maintenance of mature spine morphology with relatively slow kinetics (>30 min). Consistently, nocodazole

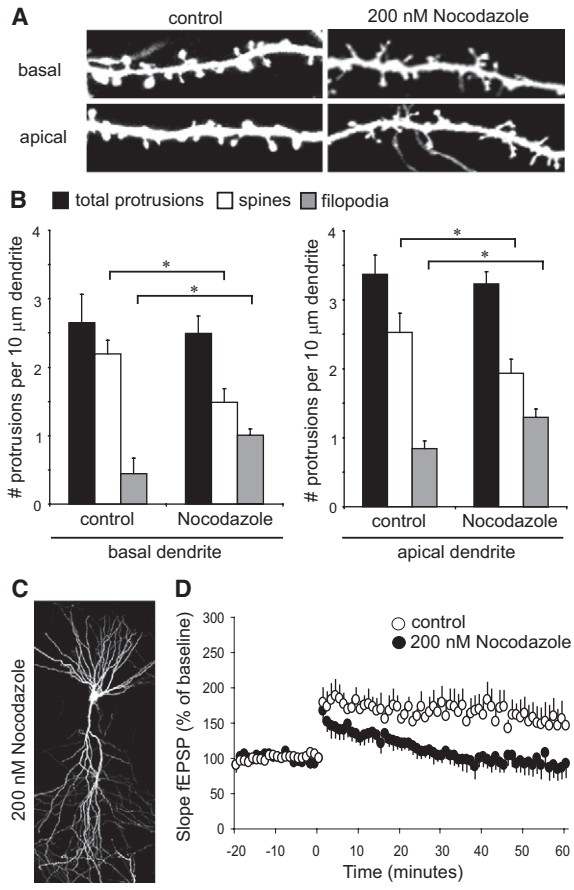

Figure 3. Dynamic MTs Are Required for Synaptic Transmission and Spine Maintenance in Hippocampal Slices

(A) Representative images of basal and apical dendrites from CA1 pyramidal neurons in hippocampal slice cultures from P7 rats transfected with GFP and incubated for 4 hr with 200 nM nocodazole.

(B) Quantification of number of protrusions per 10 μm basal and apical dendrites in pyramidal neurons treated as in (A). Histogram shows mean ± SEM, *$p < 0.05$.

(C) Representative image of CA1 pyramidal neuron in hippocampal slice cultures from P7 rats transfected with GFP and incubated for 4 hr with 200 nM nocodazole. Scale bar, 10 μm.

(D) Hippocampal long-term potentiation induced by high-frequency stimulation. Mouse hippocampal slices were treated with vehicle (control) or 200 nM nocodazole for 1 hr before and during recording. Subsequently, fEPSPs were recorded at 0.0166 Hz from CA1 dendritic fields upon Schaffer Collateral stimulation. After 20 min of baseline recordings, slices were stimulated using high-frequency stimulation (1 s at 100 Hz) followed by 60 min of fEPSP recording at 0.0166 Hz.

washout for 3 hr restored normal spine morphology (Figures S3A–S3C), indicating that the effect on spines is reversible and most likely due to reduced MT dynamics.

The effect of nocodazole on spine shape might be explained by the loss EB3 from MT tips. To test this idea, we used RNA interference (RNAi) to suppress endogenous EB3. Hippocampal neurons transfected at DIV 14 for 4 days with EB3-shRNA (Figure 1) did not significantly affect the number of protrusions but resulted in a spine phenotype similar to that induced by nocodazole treatment; namely, a loss of mushroom-headed spines and an increase of thin, long filopodia-like spines (Figures 4A–4C). In contrast, overexpression of EB3-GFP induced a robust increase in the number of mushroom spines (Figures 4A–4C), suggesting that increased MT targeting might change spine morphology. No effect on spines could be seen with expression of other MT binding proteins, such as CLIP-115 and MAP2c or treatments with 2 μM of the MT stabilizing drug Taxol (Figures S3D–S3F). Moreover nocodazole treatment prevented the EB3-GFP effect on spines (Figures S3G–S3I), implying that the interaction of EB3 with MTs is necessary for spine growth.

EB3-GFP Entry in Spines Accompanies Spine Enlargement

To explore the relationship between EB3-GFP entry and spine growth, the spine area of preexisting spines was monitored for extended periods (>10 min) before and after EB3-GFP comet entry. On average 10% ± 7% (mean ± SD, n = 227 spines in 12 neurons) of the spines were targeted by EB3-GFP within a 10 min time frame. We rarely observed a decrease in spine size correlated with EB3-GFP entry, whereas often spine growth was observed after EB3-GFP entry (Figures 5A–5C; Movie S4). Detailed analysis of several events (n = 20 spines) revealed that 60% of the spines have a >20% increase in spine growth upon EB3 entry under basal culture conditions (Figure 5F). In contrast, control spines that existed throughout the imaging without EB3 entry events show only a slight variation in spine size; only 15% of the control spines showed >20% increase in spine area. Typically, the increase in spine size is correlated with just one or two entries of EB3-GFP (67% of spines) (Figure 5E), or occasionally repeated movements of EB3-GFP in the same spine (Figure 5D). We did not find a correlation between the number of comet entries (within 3 min) and subsequent changes in spine size (data not shown). Consistent with the changes in spine shape found in fixed cells (Figures 4A–4C), these results demonstrate that the entry of EB3-GFP decorated MT tips into dendritic spines is associated with spine growth, further indicating a role for MT targeting in spine morphological plasticity.

EB3 Regulates Actin Dynamics within Spines

Since +TIPs have been implicated in the regulation of actin remodeling in various systems, we next tested if altered spine shape was correlated with actin reorganization. Consistent with previous studies, in control DIV 17 neurons, F-actin appeared as patches and puncta along the dendrites and was enriched in the heads of dendritic spines (Figure 4A). Nocodazole treatment or expression of EB3-shRNA resulted in a pronounced loss of F-actin from dendritic protrusions (Figures 4A and 4D). Conversely, expression of EB3-GFP increased F-actin abundance (Figures 4A and 4D).

To extend this observation, we treated control and EB3 knockdown neurons with two actin-directed drugs, latrunculin B and jasplakinolide, that are known to shift the equilibrium toward G-actin and F-actin, respectively (Okamoto et al., 2004). Treatment of EB3-shRNA-transfected neurons with latrunculin B (10 μM, 2 hr) showed a further increase in filopodia and decrease in spines compared to nontreated EB3-deficient or control

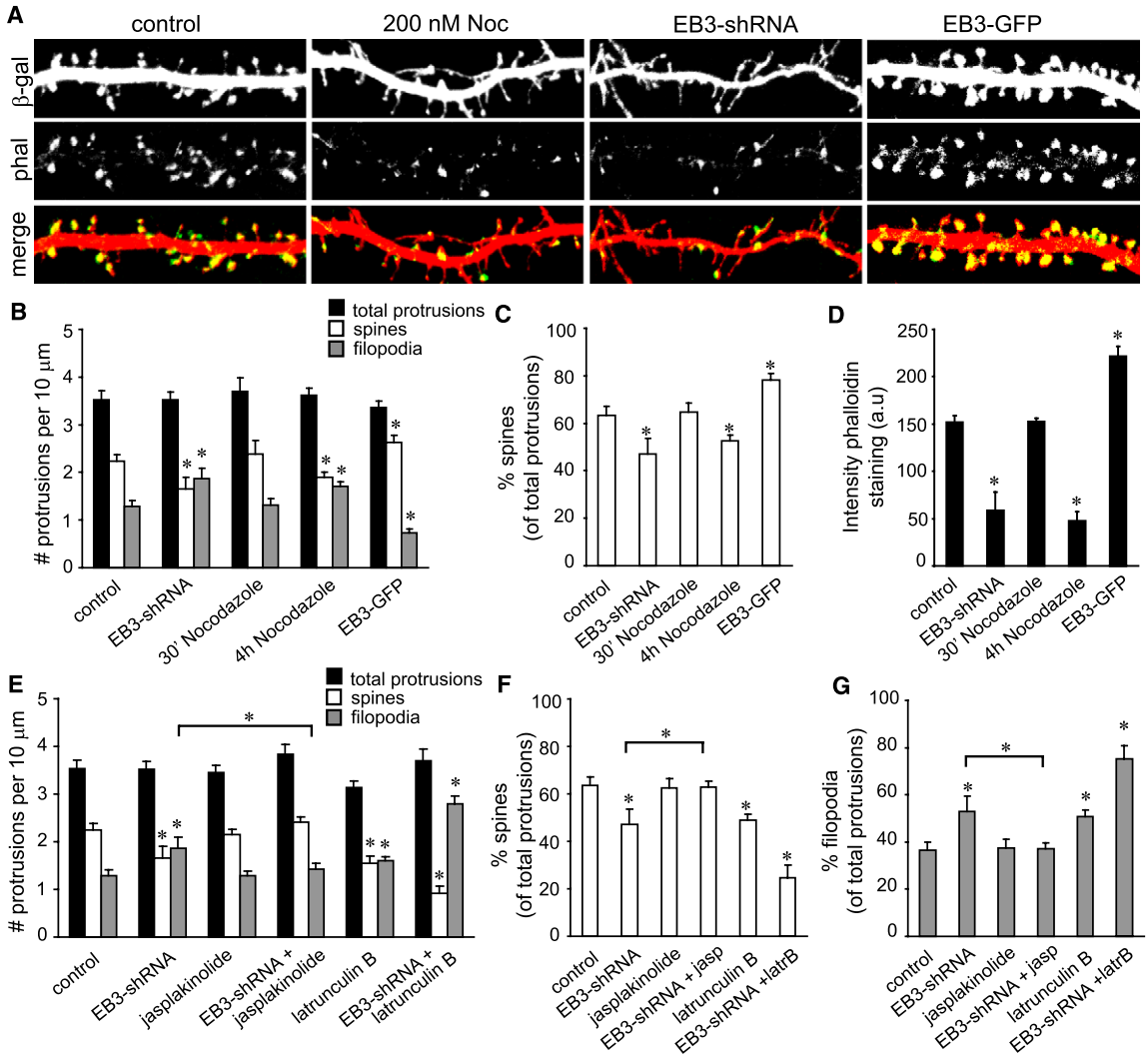

Figure 4. MT Plus-End-Bound EB3 Regulates Actin Dynamics within Spines

(A) High-magnification images of dendrites of hippocampal neurons transfected at DIV 13 for 4 days with the control pSuper vector, EB3-shRNA, or EB3-GFP or treated with 200 nM nocodazole for 4 hr and double-labeled with phalloidin-A594 and the cotransfected β-gal (red) to visualize the neuronal morphology.

(B) Quantification of number of protrusions per 10 um dendrites in hippocampal neurons transfected at DIV 13 with the control pSuper vector, EB3-shRNA, or EB3-GFP or treated with 200 nM nocodazole for 30 min or 4 hr. Histograms show mean ± SEM, *$p < 0.05$.

(C) Percentage of spines (C) of hippocampal neurons transfected and treated as indicated in (B).

(D) Quantification of phalloidin immunostaining intensities (as arbitrary units) in dendrites of hippocampal neuron transfected and treated as indicated in (B).

(E) Quantification of the number of protrusions per 10 μm dendrites in hippocampal neurons transfected at DIV 13 with control pSuper vector or EB3-shRNA, either untreated or treated with 10 μM latrunculin B or 10 μM jasplakinolide for 2 hr.

(F and G) Percentage of spines (F) and filopodia (G) in hippocampal neurons transfected and treated as indicated in (E).

neurons (Figures 4E–4G). On the other hand, treatment of EB3-depleted neurons with jasplakinolide (10 μM, 2 hr) rescued the EB3 knockdown phenotype (Figures 4E–4G). These data support the idea that the MT plus-end-bound EB3 regulates actin dynamics within dendritic spines.

p140Cap Binds to EB3 and Associates with Growing MT Ends

To investigate the mechanism by which EB3 influences the actin cytoskeleton in spines, we searched for EB3 binding partners in hippocampal neurons. We performed glutathione S-transferase (GST) pull-down assays with extracts from primary hippocampal neurons (DIV 21) using GST-EB3 fusions and analyzed the isolated proteins by mass spectrometry. Among the proteins which were highly enriched in the GST-EB3 pull down and not present in the control GST pull down, were several known +TIP partners of EB3, such as CLIP-115 and CLASP2 (reviewed in Jaworski et al., 2008; Lansbergen and Akhmanova, 2006) (Table S1). The most significant novel hit in this experiment was p140Cap (also known as SNIP; SNAP-25 interacting protein) (Chin et al., 2000) (Figure 6A; Table S1). p140Cap is a recently discovered Src-binding protein which inhibits Src kinase activity, regulates

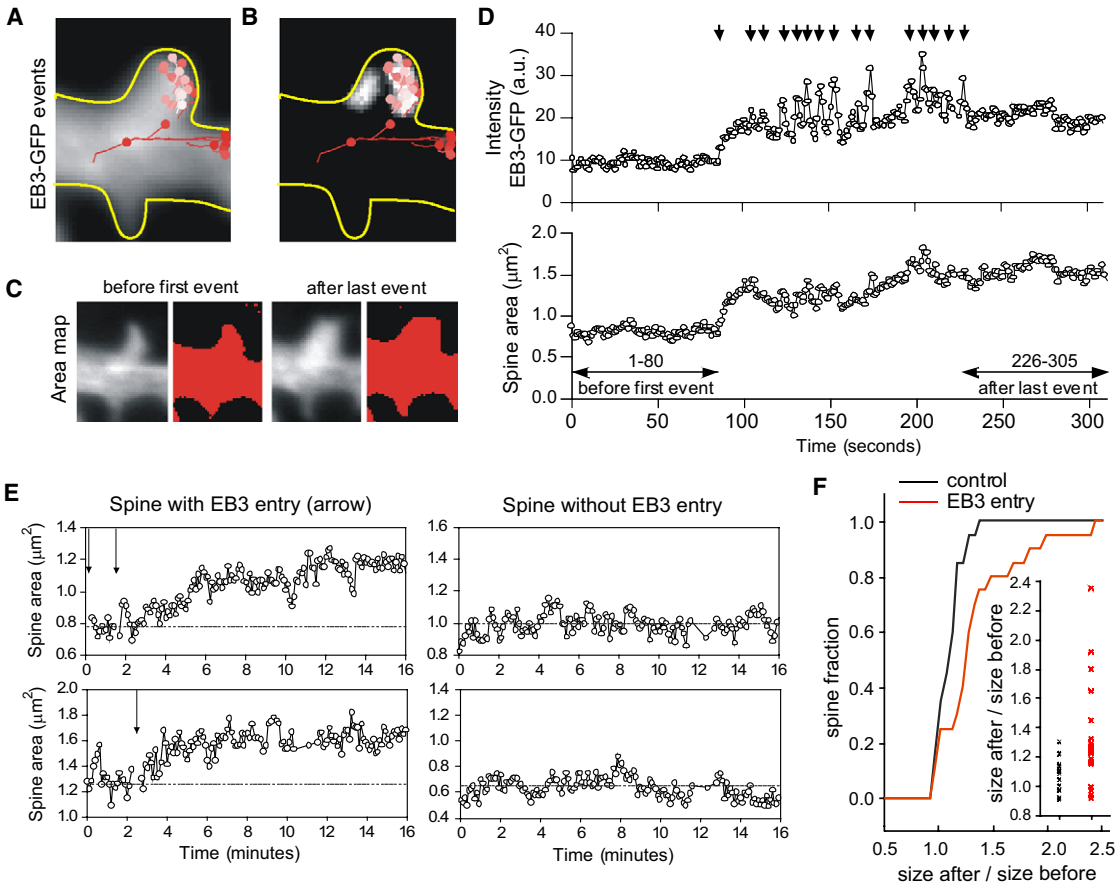

Figure 5. EB3-GFP Entry into Dendritic Spines Is Associated with Spine Growth

(A) Average spine morphology obtained by averaging the time-lapse recording, overlaid with the trajectories of EB3-GFP comets detected during the recording. Progression of time is color coded from dark to light and circles indicate end of trajectories.

(B) Image representing the intensity standard deviation per pixel, overlaid with trajectories of EB3 comets. Bright regions have varying intensities due to moving EB3-GFP comets and spine growth.

(C) Quantitative changes in spine area. Average spine area of 80 frames before/after the first/last EB3-GFP comet entering the spine, respectively. The binary image for measuring spine size is shown in red.

(D) Time trace of spine total intensity (upper panel) and spine total area (lower panel) for 300 s (5 min). Images were taken every 1 s. Arrows indicate events of entering EB3-GFP comets, corresponding with temporarily increased intensities.

(E) Examples of spine growth upon EB3-GFP comet entry. Representative traces of spine sizes with (left) or without (right) EB3 entry (depicted by arrows) over longer time (16 min). Images were taken every 2 s to resolve all EB3 entry events. Every three consecutive frames were averaged to enhance visibility.

(F) Cumulative probability distribution of the ratio of spine size before and after EB3 entry (red line, n = 20), compared with control spines without EB3 entry (ratio of spine size after 10 and 5 min, see methods. n = 20).

the actin cytoskeleton and suppresses tumor growth (Di Stefano et al., 2007). To confirm the interaction of p140Cap with EB3 and other EB family members, we performed GST pull down assays with extracts of HEK293 cells expressing GFP alone or GFP-p140Cap. While GFP alone did not interact with any GST fusions (data not shown), the full-length p140Cap (amino acids 1–1216) strongly associated with all members of the EB family and GST-EB1 C terminus but not with GST alone or GST-EB1 N terminus (Figures 6B and 6C). This is in line with the data on other EB binding partners, which all bind to the C-terminal portion of the protein (reviewed in Jaworski et al., 2008; Lansbergen and Akhmanova, 2006). By expressing truncated versions of GFP-p140Cap (Figure 6A), we mapped the minimal EB-binding region of p140Cap. While the large N-terminal part of p140Cap (amino acids 1–1164) did not interact with any EB proteins, the short 92 amino acid C-terminal region of p140Cap (amino acids 1124–1216) bound to all three GST-EB fusions (Figure 6B). It is likely that the positively charged S/P-rich region within the C terminus of p140Cap is involved in associating with the EB C terminus, because similar domains within other EB-binding partners have also been implicated in this function (Jaworski et al., 2008; Lansbergen and Akhmanova, 2006). The interaction between EB3 and p140Cap under physiological conditions was confirmed by coimmunoprecipitation of endogenous proteins from synaptosome fractions (Figure 6D). In the same experiment, p140Cap was also able to coimmunoprecipitate Src kinase (Figure 6D), consistent with the data from tumor cells (Di Stefano et al., 2007).

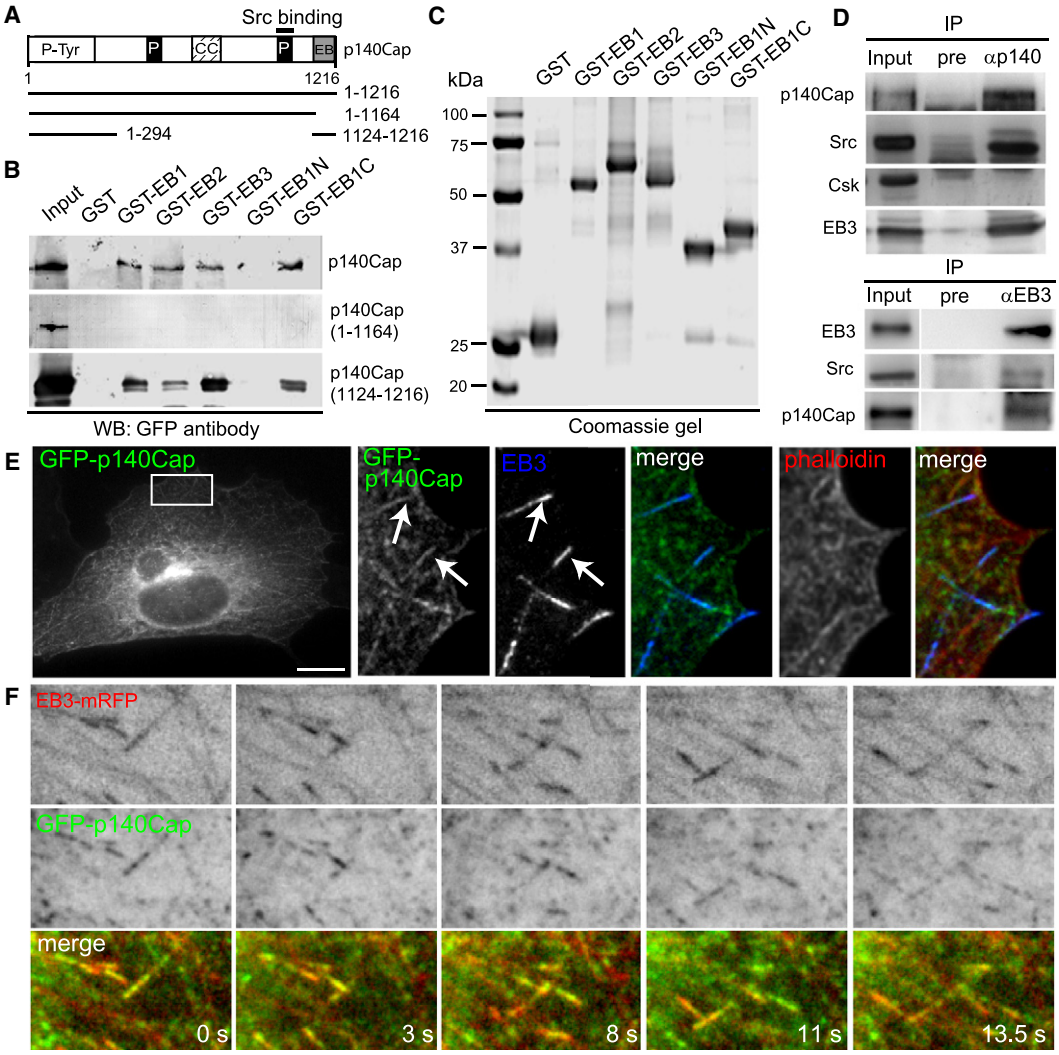

Figure 6. p140Cap Interacts with EB3

(A) Diagram of p140Cap structure and mutant constructs (GFP tag was placed at N terminus). P-Tyr, stretch of phosphorylated tyrosine residues; P, proline-rich domain; CC, coiled coil; EB, minimal EB-binding domain. The second proline-rich region binds to Src kinase.

(B) GST pull-down assays with the indicated GST fusions and extracts of HEK293 cells overexpressing GFP-p140Cap, GFP-p140Cap(1-1164), or GFP-p140Cap(1124-1216). GFP fusions were detected by western blotting with antibodies against GFP.

(C) Coomassie-stained gels are shown for GST fusions.

(D) Immunoprecipitation from mouse crude synaptosomes with anti-p140Cap or anti-EB3 antibodies and preimmune serum (pre) as negative control. Three milligrams of the crude synaptosomal fraction (input = 50 μg) were immunoprecipitated and analyzed by western blotting for indicated proteins.

(E) COS-7 cells were transfected with GFP-p140Cap (green), methanol fixed and stained for endogenous EB3 (blue) and F-actin, by phalloidin-A594 (red). The insets show enlargements of the boxed area. The merge of GFP-p140Cap and endogenous EB3 (green/blue) and GFP-p140Cap/EB3/F-actin (green/blue/red) is shown. Scale bar, 10 μm.

(F) Simultaneous imaging of GFP-p140Cap (green) and EB3-mRFP (red) in transfected MRC5-SV cells. Successive frames are shown. Time is indicated in the merge panel.

Next, we investigated the localization of GFP-p140Cap in non-neuronal cells. As previously observed (Di Stefano et al., 2007), GFP-p140Cap localized throughout the cytoplasm and showed a modest colocalization with F-actin (Figure 6E). In addition, we observed GFP-p140Cap-positive comet-like structures, which coincided with some of the MT plus ends labeled for endogenous EB3 (Figure 6E). Further indications of an interaction between the two proteins were provided by coexpression of GFP-p140Cap and EB3-mRFP. At low expression levels, EB3-mRFP colocalized with GFP-p140Cap on MT plus ends (Figure S4A). However, when EB3 was distributed evenly along the MTs due to overexpression, GFP-p140Cap also decorated the whole MT lattice (Figure S4B).

The ability of p140Cap to associate with growing MT ends was further confirmed by simultaneous dual color live imaging of GFP-p140Cap and EB3-mRFP: GFP-p140Cap was observed

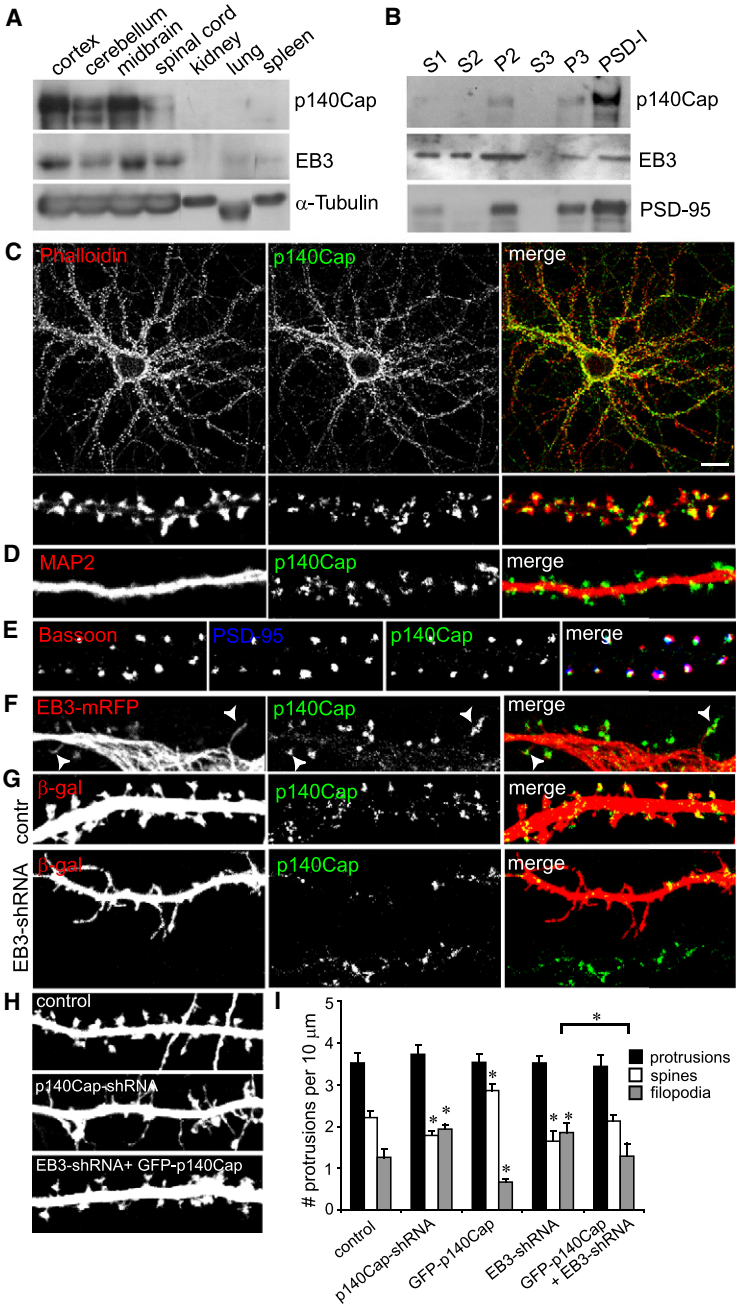

Figure 7. p140Cap Localizes to Synapses and Is Required for Spine Maintenance

(A) Tissue expression of p140Cap. Mouse tissue homogenates (20 μg of protein/lane) were analyzed by SDS-PAGE and immunoblotting using anti-p140Cap and anti-EB3 antibodies. α-Tubulin as is used as a loading control.

(B) Enrichment of p140Cap in the PSD fraction. Hippocampal neurons at DIV 21 were homogenized, fractionated by differential centrifugation, and analyzed by immunoblotting using anti-p140Cap, anti-EB3 and anti-PSD-95 antibodies.

(C) Representative images of rat hippocampal neurons (DIV 17) labeled with rabbit anti-p140Cap antibody (green) and phalloidin-A594 (red), to visualize F-actin. Dendritic segments (lower panels) are enlarged to show the colocalization of p140Cap and F-actin in spines. Scale bar, 10 μm.

(D) Dendrites of hippocampal neurons labeled with rabbit anti-p140Cap antibody (green) and mouse anti-MAP2 (red).

(E) Dendrites of hippocampal neurons triple labeled with rabbit anti-p140Cap antibody (green), guinea pig anti-PSD-95 antibody (blue), and mouse anti-Bassoon (red).

(F) Hippocampal neurons transfected at DIV 13 with EB3-mRFP and labeled with mouse anti-p140Cap (red). Arrowheads indicate colocalized EB3-mRFP and p140Cap.

(G) Representative images of hippocampal neurons transfected at DIV 13 with control pSuper vector or EB3-shRNA and double labeled with anti-p140Cap (green) and cotransfected β-gal (red).

(H) Representative images of hippocampal neurons transfected at DIV 13 with control pSuper vector, p140Cap-shRNA, or EB3-shRNA and GFP-p140Cap and stained for cotransfected β-gal to highlight neuronal morphology.

(I) Quantification of number of protrusions per 10 μm dendrites in hippocampal neurons transfected at DIV 13 with control pSuper vector, p140Cap-shRNA, GFP-p140Cap, EB3-shRNA, and a combination of EB3-shRNA and GFP-p140Cap. Error bars indicate SEM, *$p < 0.05$.

as small granular particles that showed diffusive behavior and concentrated at EB3-positive growing MT ends (Figure 6F; Movie S5). These data indicate that, similar to other EB-binding partners, p140Cap can behave as a +TIP.

p140Cap Localizes to Synapses in Hippocampal Neurons

Western blot analyses showed that both p140Cap and EB3 are predominantly expressed in the central nervous system and present in different brain regions (Figure 7A), consistent with previous studies (Chin et al., 2000; Di Stefano et al., 2004; Nakagawa et al., 2000). Several PSD proteome studies have identified p140Cap/SNIP as an abundant constituent of the PSD (Dosemeci et al., 2007; Peng et al., 2004; Trinidad et al., 2006), but its function at the synapse has not yet been studied. Our biochemical fractionation experiments confirmed the presence of p140Cap in synaptosomal membrane fractions and its enrichment in PSD fractions, similar to core PSD components such as PSD-95 (Figure 7B). In agreement with the biochemical experiments, immunofluorescent staining of p140Cap in cultured neurons revealed granular puncta of different size that were distributed along dendrites and concentrated within F-actin-enriched dendritic spines (Figure 7C). The p140Cap puncta were not restricted to the spine head but often extended toward the dendritic shaft, suggesting that the zone of p140Cap accumulation might include the neck of the spine. More than 70% of the dendritic p140Cap showed overlap with the postsynaptic marker PSD-95 and presynaptic protein Bassoon (Figure 7E). The punctate distribution of p140Cap showed little colocalization with MTs in the dendritic shaft, as revealed by costaining with MAP2 (Figure 7D). Furthermore, very little overlap of p140Cap and EB3 positive MT plus end in the dendritic shaft could be observed, in spite of the marked colocalization between mRFP-EB3 and p140Cap within the spines (Figure 7F). Thus,

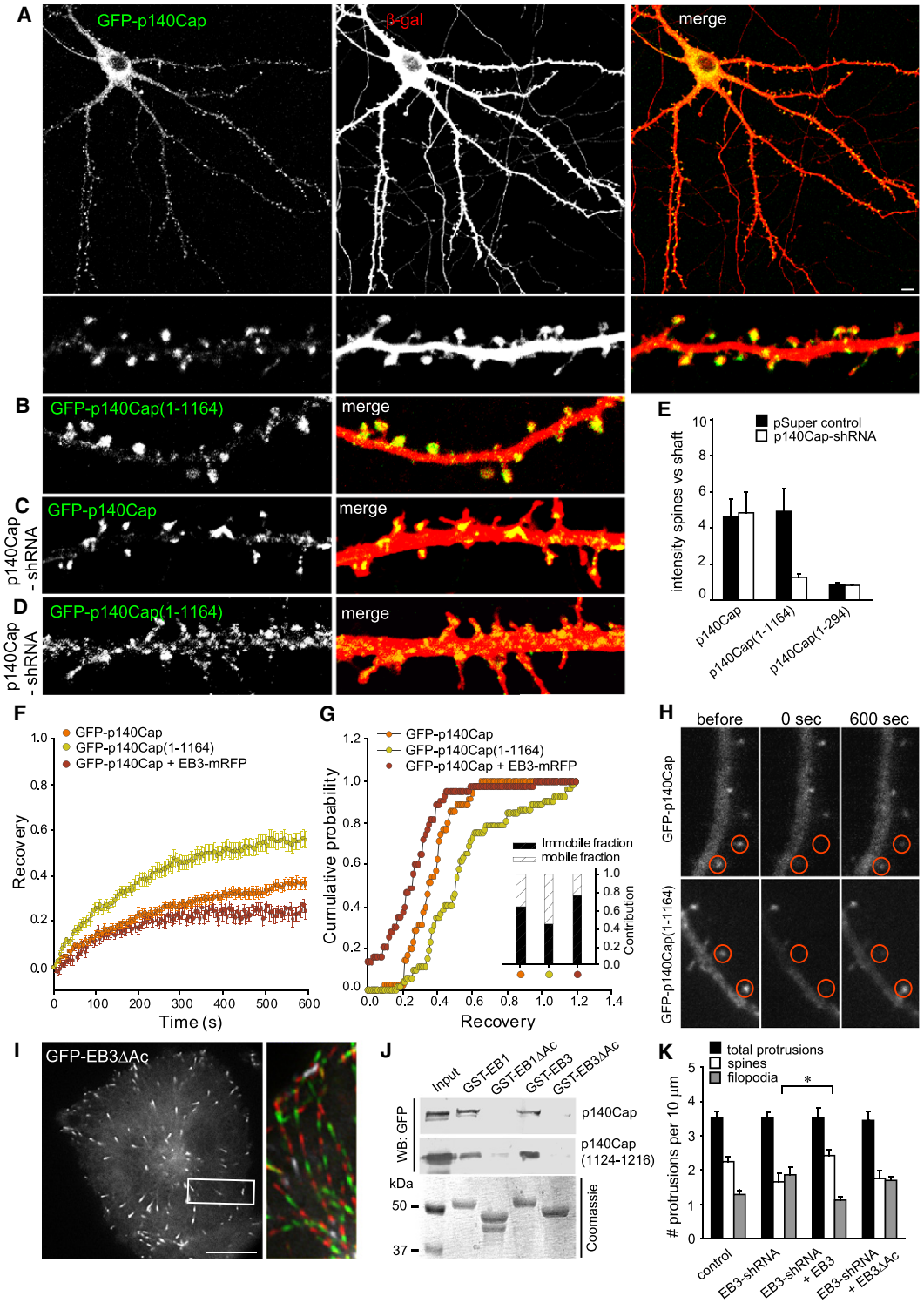

Figure 8. EB3 Is Required for p140Cap Distribution in Hippocampal Neurons

(A–D) Representative images of hippocampal neurons cotransfected at DIV 13 with full-length GFP-p140Cap or GFP-p140Cap(1-1164) with pSuper control vector (A and B) or p140Cap-shRNA (C and D) and labeled for cotransfected β-gal (red). Dendritic segments are enlarged to show the distribution of GFP-140Cap. Only the merge is shown in color. Scale bar, 10 μm.

(E) Quantification of GFP-140Cap spine targeting. Numbers indicate the ratio of fluorescence intensity in spines versus dendritic shafts of each indicated p140Cap construct with pSuper control vector or p140Cap-shRNA (mean ± SEM), as index of spine targeting.

p140Cap appears to be a synaptic protein which concentrates in spines and may interact with EB3-labeled MT tips entering the spines.

Loss of p140Cap Causes a Decrease in Spine Density

To investigate the role of p140Cap in dendritic spine morphology, we knocked down endogenous p140Cap using plasmid-based RNAi. Transfection of the p140Cap-shRNA construct caused an ~70% reduction in immunostaining for p140Cap in dendrites and the cell body (Figures S5A and S5B) but induced no change in other proteins, such as MAP2 (data not shown). Knockdown of p140Cap caused a significant decrease in the number of spines and an increase in the number of filopodia, while the total protrusion density was unchanged (Figures 7H and 7I). The density of F-actin in dendrites of p140Cap-deficient neurons was significantly diminished (data not shown), similar to the EB3 knock-down neurons. In contrast, GFP-p140Cap overexpression caused an opposite effect on the ratio between spines and filopodia and an increase in F-actin abundance (Figures 7H and 7I). Taken together, these results imply that p140Cap is involved in stabilization of mushroom-like spines.

EB3 and p140Cap Cooperate in Regulating Spine Morphology

Since EB3 and p140Cap interact with each other and their depletion causes similar spine phenotypes, the two proteins may act in the same pathway. To test this possibility, we investigated p140Cap localization in EB3-deficient neurons. We transfected neurons at DIV 13 with EB3-shRNA; 4 days later we observed that the staining of p140Cap in the dendritic protrusions was significantly reduced (Figure 7G). Quantification revealed a 75% reduction in p140Cap protrusion staining intensity in EB3 knockdown neurons compared to control neurons.

To obtain insight in to how EB3 might regulate p140Cap localization, we determined whether the EB3-binding domain of p140Cap is required for its targeting to spines. Neurons were transfected with full-length p140Cap or its truncated versions, GFP-p140Cap(1-1164), that lacks the EB3-binding site, and GFP-p140Cap(1-294) that also lacks the Src-binding site (Figure 6A). GFP-p140Cap(1-1164) accumulated in spines as efficiently as the full-length protein (Figures 8A and 8E), while GFP-p140Cap(1-294) lost its spine targeting (Figure 8E). Since p140Cap has a coiled-coil in the middle of the protein and could interact with itself, endogenous p140Cap may stabilize exogenous p140Cap protein within the spines. To test this hypothesis, we cotransfected neurons at DIV 13 with p140Cap-shRNA and full-length GFP-p140Cap or GFP-p140Cap(1-1164); 4 days later we observed that the accumulation of GFP-p140Cap(1-1164) in the dendritic protrusions was significantly reduced compared to full-length GFP-p140Cap (Figures 8C–8E). To interfere with the specific interaction between EB3 and p140Cap, we overexpressed the EB3-binding C terminus of p140Cap (1124-1216) (Figures S4B) and observed a significant decrease in the number of mushroom-shaped spines (Figures S5D and S5E). In addition, expressing a 23 aa C-terminally truncated EB3 construct (GFP-EB3ΔAc), which is unable to bind to p140Cap (Figure 8J) but can bind to MT plus ends and regulate MT dynamics (Figure 8I), does not increase the number of mushroom spines compared to full-length EB3-GFP (Figures S3D–S3F). Furthermore, full-length EB3-GFP but not GFP-EB3ΔAc is able to rescue the EB3 knockdown phenotype (Figure 8K). Together these data indicate that the EB3-p140Cap interaction is necessary for regulating spine morphology.

We hypothesized that the EB3-binding region might affect the turnover of p140Cap in spines. Fluorescence recovery after photobleaching (FRAP) revealed that on average, full-length GFP-p140Cap fluorescence recovers to 36% ± 2% (mean ± SEM, n = 35 spines) of prebleach intensity with an average recovery half-time of $\tau_{1/2}$ = 148 ± 11 s (mean ± SEM) (Figure 8F). Fitting a single-exponential recovery curve to the average recovery time trace yielded similar results ($\tau_{1/2}$ = 153 ± 36 s, Recovery level R_{final} = 38% ± 4%), indicating that there are two p140Cap populations; one mobile fraction with a turnover time of minutes and another, more stable fraction that turns over on a timescale much longer than 15 min (Figures 8G and 8H). FRAP analysis of GFP-p140Cap(1-1164) showed not much change in the recovery half-time ($\tau_{1/2}$ = 125 ± 9 s, mean ± SEM, n = 52 spines), but a much higher recovery level than full-length GFP-p140Cap (R_{final} = 55% ± 4%, mean ± SEM), indicating that the fraction of stably incorporated p140Cap has decreased by almost 30% (Figures 8F–8H). Coexpression of GFP-p140Cap and EB3-mRFP revealed a lower GFP recovery level compared to p140Cap alone (R_{final} = 23% ± 3%, mean ± SEM, n = 43 spines) (Figures 8G and 8H). Although we cannot exclude that other factors also influence p140Cap turnover in spines, the FRAP data reveal that the EB3 interaction is important for regulation of p140Cap accumulation within spines.

Next, we tested whether p140Cap acts up- or downstream of EB3 in regulating spine shape. While overexpression of GFP-p140Cap fully restored the number of mushroom-shaped spines in EB3 depleted neurons (Figures 7H and 7I), GFP-EB3

(F) Averaged time traces of fluorescence recovery after photobleaching for full-length GFP-p140Cap (orange circles, 35 spines), GFP-p140Cap(1-1164) (green circles, 52 spines) or GFP-p140Cap coexpressing EB3-mRFP (red circles, 43 spines). Error bars show SEM.
(G) Cumulative probability distribution of the recovery levels 595 s after bleaching. Inset shows the average size of the mobile and immobile fractions of GFP-p140Cap, GFP-p140Cap(1-1164) and GFP-p140Cap plus EB3-mRFP.
(H) Examples of the fluorescence distribution and intensity of GFP-p140Cap and GFP-p140Cap(1-1164) before, directly after and 600 s after bleaching the spines indicated with circles.
(I) CHO cells were transfected with GFP- EB3ΔAc and imaged every 500 ms. The GFP- EB3ΔAc positive growing MT ends are color coded for each fifth frame (2.5 s). Frame 1 is show in white (at left) and every subsequent fifth frames is alternately colored red and green in the enlargement (at right). Scale bar, 10 μm.
(J) GST pull-down assays with the indicated GST fusions and extracts of HEK293 cells overexpressing GFP-p140Cap and GFP-p140Cap(1124-1216). GFP fusions were detected by western blotting with antibodies against GFP. Coomassie-stained gel is shown for GST fusions.
(K) Quantification of the number of dendritic protrusions per 10 μM in hippocampal neurons transfected at DIV 13 with empty vector (control), EB3-shRNA alone, or EB3-shRNA with EB3 or EB3ΔAc. Error bars indicate SEM, *p < 0.05.

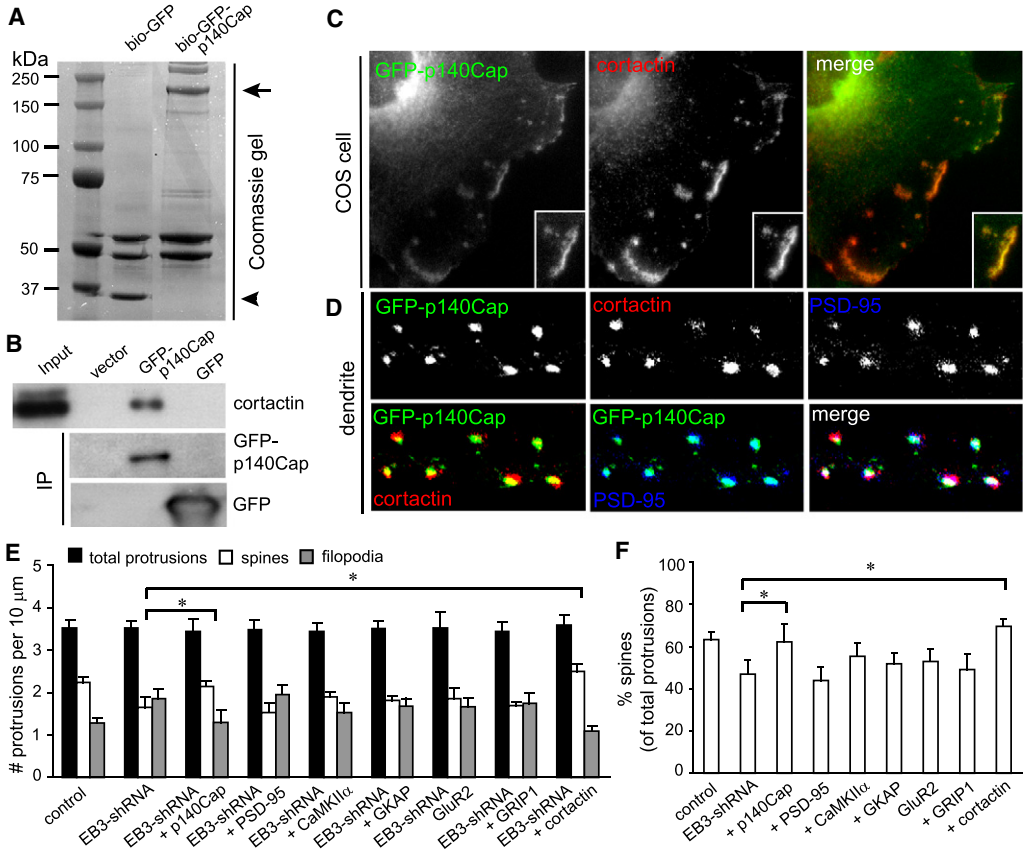

Figure 9. p140Cap Interacts with Cortactin

(A) Streptavidin pull-down assays were performed with lysates of HeLa cells coexpressing bio-GFP-p140Cap or bio-GFP together with BirA. Proteins bound to streptavidin beads were analyzed on a Coomassie-stained gel. The arrowhead and the arrow indicate bio-GFP and bio-GFP-p140Cap protein bands, respectively.

(B) Immunoprecipitations from extracts of transfected HeLa cells with the indicated constructs and probed for cortactin.

(C) COS-7 cells were transfected with GFP-p140Cap, formaldehyde fixed and stained for endogenous cortactin (red). The insets show enlargements of cortactin and p140Cap colocalization at cortical membrane ruffles.

(D) Dendrites of hippocampal neurons triple labeled for transfected GFP-p140Cap (green), rabbit anti-cortactin (red), and guinea pig anti-PSD-95 antibody (blue).

(E) Quantification of number of protrusions per 10 μm dendrite in hippocampal neurons transfected at DIV 13 with control pSuper vector, EB3-shRNA, or EB3-shRNA plus the indicated constructs. Histograms show mean ± SEM, *$p < 0.05$.

(F) Percentage of spines of hippocampal neurons transfected with constructs indicated in (E).

expression was unable to rescue the p140Cap phenotype (data not shown). Taken together, our data suggest that EB3 located at the growing MT ends regulates the distribution of p140Cap, which in its turn controls dendritic spine morphology.

p140Cap Binds to Cortactin

While EB3-positive MT plus ends regulates the stability of p140Cap and modulates actin dynamics within dendritic spines, we wanted to gain a better understanding of how EB3/p140Cap regulates the actin cytoskeleton. We next searched for p140Cap binding partners using pull-down assays combined with mass spectrometry. Biotinylation and GFP-tagged p140Cap (bio-GFP-p140Cap) and bio-GFP as a control were transiently coexpressed in HeLa cells together with the protein-biotin ligase BirA and isolated with streptavidin beads (Figure 9A). Mass-spectrometry analysis of the whole bio-GFP-p140Cap lane revealed several actin-related proteins, including Crk (Bougneres et al., 2004), CD2-associated protein (CD2AP) (Lynch et al., 2003), cortactin (Wu and Parsons, 1993), and Shank (Naisbitt et al., 1999) that were not present in the control lane (Table S2). Interestingly, all the identified proteins have previously been shown to interact with cortactin (Ammer and Weed, 2008), suggesting that p140Cap in HeLa cells associates with a cortactin-containing protein complex. Additional bio-p140Cap mass-spectrometry experiments using MCF7 and brain extract all identified cortactin while the other cortactin interacting proteins were not found (data not shown). The interaction between p140Cap and cortactin was confirmed by immunoprecipitation experiments (Figure 9B). Cortactin is an F-actin-binding protein implicated in the stabilization and branching of actin filaments and shown to concentrate with F-actin at cortical membrane in nonneuronal cells (Wu and Parsons, 1993) and dendritic spines of cultured hippocampal neurons (Hering and Sheng, 2003). Expression of GFP-p140Cap revealed colocalization with cortactin at membrane

ruffles and lamellipodia in COS-7 cells (Figure 9C) and dendritic spines positive for the postsynaptic marker PSD-95 (Figure 9D). It has been shown that loss of cortactin results in a decrease of F-actin staining and reduction of dendritic spines (Hering and Sheng, 2003), similarly to the effects seen with EB3 and p140Cap knockdown. We confirmed the loss-of-function experiments by using cortactin shRNA (data not shown) and tested whether cortactin regulates spine morphology downstream of EB3 in controlling spine shape. Overexpression of myc-tagged cortactin fully restored the number of mushroom-shaped spines in EB3 depleted neurons, similarly to expression of GFP-p140Cap (Figures 9E and 9F). In contrast no rescue of the EB3 knockdown spine phenotype could be seen by overexpressing other major postsynaptic proteins, such as PSD-95, CaMKIIα, GKAP, GluR2, or GRIP1 (Figures 9E and 9F). These findings show that p140Cap and its interacting partner cortactin specifically rescue the EB3 depletion phenotype and strengths the link between EB3, p140Cap and the actin cytoskeleton.

DISCUSSION

In this study we describe a structural and functional interplay between dendritic MTs and actin cytoskeleton within spines. Unexpectedly, dynamic MTs can penetrate into dendritic spines and are required to maintain their shape. EB3-bound MT plus ends modulate spine shape by affecting the abundance of F-actin. This view is supported by the observation that EB3 knockdown phenotype is rescued by jasplakinolide, a drug that promotes actin polymerization. These findings are in line with genetic studies in yeast where +TIPs regulate cell shape by affecting the actin cytoskeleton (Basu and Chang, 2007). Furthermore, we identified an EB3 binding partner, p140Cap, a regulator of Src kinase activity shown to be involved in controlling actin organization (Di Stefano et al., 2007). In this study we also found that p140Cap binds to the Src kinase substrate and F-actin binding protein cortactin (Wu and Parsons, 1993). Overexpression of p140Cap or cortactin rescues the EB3 depletion phenotype. The interactions of EB3-positive MT plus-ends, p140Cap and cortactin may therefore represent a link between the local signaling of MTs and the actin cytoskeleton within the dendritic spines.

Regulation of Spine Morphology by Dendritic MTs

It is widely accepted that in dendrites of mature neurons, the cytoskeletal microdomains are spatially separated: actin filaments are predominately concentrated in spines while MTs are restricted to the dendritic shaft and rarely observed within dendritic spines (Kaech et al., 2001; Westrum et al., 1980). This conclusion is mainly based on ultrastructural studies as well as live imaging experiments using MAP2-GFP, which revealed that stable MTs are absent from spines (Kaech et al., 2001; Landis and Reese, 1983). In this study, we particularly focus on dynamic MTs by using EB3-GFP and show that growing MTs can enter dendritic spines. In accord with these data it was shown previously that the large dendritic spines of CA3 pyramidal neurons frequently contain MTs (Chicurel and Harris, 1992) and that some MT components and associated proteins are present in spines and PSD fractions (Sheng and Hoogenraad, 2007; van Rossum and Hanisch, 1999). Thus, it seems that stable MTs are predominantly present as bundles in dendritic shafts whereas dynamic MTs can enter dendritic spines.

Furthermore, we show that entry of dynamic MT plus ends is physiologically relevant. First, EB3-GFP entry in spines frequently accompanies spine enlargement. Second, a low dose of nocodazole abolishes EB3 accumulation at MT tips and leads to changes in spine morphology and synaptic transmission. Third, reduction of EB3 expression decreases F-actin staining and spine size, whereas EB3 overexpression correlates with an increase in polymerized actin and the number of mushroom-like spines. Fourth, a binding partner of EB3, p140Cap, colocalizes with F-actin in spines and its distribution is influenced by EB3 expression. We propose a model in which dynamic EB3-labeled MT ends grow into dendritic spines and influence their morphology by controlling the actin cytoskeleton by acting, at least in part, through p140Cap.

The functions of dynamic MT penetration in spines described here may extend beyond the regulation of the actin cytoskeleton. MTs within spines may be important for organizing membrane traffic and could reflect the need for cargo delivery to the postsynaptic site, analogous to the accumulation of synaptic vesicles in axonal growth cones (Dent and Gertler, 2003). It is generally believed the synaptic cargo travels along the MT transport system in the dendrite shaft and switches to the actin-dependent myosin motor system to reach the postsynaptic membrane (Kennedy and Ehlers, 2006). However, with our finding that MTs grow into spines, it is possible that cargos are also transported by MT-dependent motors toward synaptic sites (Hirokawa and Takemura, 2005; Kneussel, 2005). Furthermore, additional studies are required to determine whether neuronal activity or local calcium influx influences MTs dynamics within dendritic spines.

The Functional Significance of the EB3-p140Cap Interaction

Recent studies in various organisms have provided strong evidence that EB family proteins are conserved key molecules at growing MT plus ends. The localization of most, if not all, other plus-end tracking proteins is influenced by the presence of EBs at the MT plus-ends (Lansbergen and Akhmanova, 2006). Although p140Cap can track on EB3 labeled MT plus-ends in fibroblasts (Figure 6), the primary localization of endogenous p140Cap within hippocampal neurons is in dendritic spines. We propose that growing EB3-positive MT ends influence dendritic spine morphology by altering the turnover of p140Cap.

Several lines of evidence support this model. First, knockdown of EB3 disrupts the localization of endogenous p140Cap within the dendritic spines and FRAP analysis shows that the EB3-binding is required for p140Cap immobilization within spines. Second, p140Cap overexpression rescues the EB3 knockdown phenotype. Third, p140Cap binds EB3 via its C-terminal tail region (amino acid 1124–1216), and p140Cap(1124–1216) has a dominant-negative effect on spine morphology. Fourth, C-terminally truncated EB3 (EB3ΔAc) can interact with MT plus ends and regulate MT dynamics but it cannot bind to p140Cap and is unable to increase the number of mushroom spines in

contrast to full-length EB3; therefore, full-length EB3 and not EB3ΔAc is able to rescue the EB3 knockdown phenotype. Thus, EB3 appears to act in a MT-associated signaling pathway, in which EB3-bound growing MT ends enter the spine, "activate" p140Cap and stabilize the protein in the PSD, thereby maintaining spine and synapse size. Interestingly, an analogous model exists in epithelial cell lines where dynamic MTs are required for the integrity of cell-cell contacts (Rodriguez et al., 2003) and change the local turnover of surface E-cadherin at contact sites (Stehbens et al., 2006). Here, we propose that in hippocampal neurons EB3-decorated MT plus ends regulate the localization of p140Cap within the postsynaptic sites in order to modulate actin dynamics. Importantly, this model implies that dynamic MTs allow for the local regulation of actin dynamics at the level of individual spines, which is of key importance to understand the local changes of spine and synapse structure during plasticity and neuronal circuitry remodeling.

Cortactin Links p140Cap to the Actin Cytoskeleton

How does p140Cap regulate the actin cytoskeleton? p140Cap associates with Src kinase in synaptic membrane fractions (Figure 6D) and was shown to inhibit Src kinase activity in tumor cells (Di Stefano et al., 2007). Overexpression of constitutively active Src kinase induces filopodia-like spines (Webb et al., 2007) (and data not shown), similar to the p140Cap knockdown phenotype. In neurons, Src kinase activity is regulated by the semaphorin and/or integrin signaling pathways (Morita et al., 2006; Webb et al., 2007) to control actin dynamics (Frame et al., 2002). Thus, a likely scenario for p140Cap action involves modulation of the actin cytoskeleton through the regulation of Src kinase activity.

Here, we identified cortactin as a new binding partner of p140Cap. Cortactin is a substrate for Src kinases, implicated in the stabilization and branching of actin filaments (Ammer and Weed, 2008) and necessary for normal spine morphogenesis (Hering and Sheng, 2003). It was shown that cortactin binds F-actin and the Wiskott-Aldrich syndrome protein (WASP) and promotes actin branching via the Arp2/3 complex (Weaver et al., 2003). Moreover, the interaction between WASP and cortactin is regulated by Src kinase activity; Src phosphorylation inhibits cortactin to bind and activate WASP and reduces actin assembly (Martinez-Quiles et al., 2004). Since p140Cap inhibits Src kinase activity, the impairment of spine morphology caused by EB3 knockdown might be explained by upregulation of Src-kinase activity and inhibition of cortactin function. This model is consistent with the Src activity (Webb et al., 2007) and cortactin loss-of-function data in hippocampal neurons (Hering and Sheng, 2003).

In developing neurons, suppression of MT dynamics inhibits growth cone turning responses, as well as local actin assembly and accumulation of active Src kinases (Suter et al., 2004). It has been hypothesized that in growth cones dynamic MTs also carry signals involved in regulating Src-dependent signaling. Recently, EB1-labeled MT plus ends were found responsible for targeting Kv1 voltage-gated K^+ channels to axons and connexin hemichannels to gap junctions (Gu et al., 2006; Shaw et al., 2007). These phenomena may represent different aspects of a general molecular mechanism by which MTs position and organize regulatory factors at specific cellular locations.

EXPERIMENTAL PROCEDURES

Antibodies and Reagents

Rabbit anti-EB3 (Stepanova et al., 2003) and rabbit anti-p140Cap (Di Stefano et al., 2004) were previously described. Details of other antibodies and reagents are in the Supplemental Data.

DNA Constructs and Virus Infection

EB3-GFP was cloned in pSFV2 and packaged into Semliki Forest virus (SFV) replicons (Stepanova et al., 2003). pSuper-EB1-shRNA, pSuper-EB3-shRNA and human p140Cap-shRNA sequence are described in (Komarova et al., 2005; Di Stefano et al., 2007). GFP-p140Cap was generated by cloning human p140Cap cDNA (Di Stefano et al., 2004) into GFP tagged pGW1. For details see Supplemental Data.

Primary Hippocampal Neuron Cultures and Transfection

Primary hippocampal cultures were prepared from embryonic day 18 (E18) rat brains as described (Hoogenraad et al., 2005) and transfected using Lipofectamine 2000 (Invitrogen).

Image Acquisition, Processing, and Morphometric Analyses

Simultaneous dual color time-lapse live cell imaging and TIRFM was performed on a Nikon Eclipse TE2000E microscope with Coolsnap and QuantEM cameras (Roper Scientific). Neurons were maintained at 37°C with 5% CO_2 (Tokai Hit). FRAP experiments were performed using the scanning head 3 FRAP L5 D – CURIE (Curie Institute). For fixed neurons the dendritic protrusions were classified based on the ratio of spine head width to protrusion length. For details see the Supplemental Data.

Electrophysiological Recordings

Mouse hippocampal slices were prepared and treated with vehicle (control) or 200 nM of nocodazole. A stimulation electrode was placed in the Schaffer collateral-commissural fibers and glass microelectrodes in the CA1 dendritic layer to record fEPSP. After high-frequency stimulation (1 s at 100 Hz) synaptic responses were measured for 60 min at 0.0166 Hz. Details on the materials and methods are in the Supplemental Data.

SUPPLEMENTAL DATA

The Supplemental Data include tables, figures, and Experimental Procedures and can be found with this article online at http://www.neuron.org/supplemental/S0896-6273(08)00967-7.

ACKNOWLEDGMENTS

We thank Dr. Niels Galjart for CLIP-115 and CLIP-170 antibodies; Dr. Nicole Leclerc for GFP-MAP2c construct; and Daan Visser for generating EB3-GFP Semliki Forest virus; Nanda Keijzer for preparing primary neuronal cultures; and Karel Bezstarosti for help with mass spectrometry analyses. J.J. is supported by Polish Ministry of Science and Higher Education grant (2P04A01530) and Dutch-Polish Academy of Sciences exchange KNAW fellowship. L.C.K. is supported by the Erasmus MC fellowship program. S.M.G. is supported by Fundação para a Ciência e a Tecnologia. A.A. is supported by the Netherlands Organization for Scientific Research (NWO-VICI). C.C.H. is supported by the Netherlands Organization for Scientific Research (NWO-VIDI), European Science Foundation (European Young Investigators (EURYI) Award) and Human Frontier Science Program Career Development Award (HFSP-CDA).

Accepted: November 6, 2008
Published: January 14, 2009

REFERENCES

Akhmanova, A., and Hoogenraad, C.C. (2005). Microtubule plus-end-tracking proteins: mechanisms and functions. Curr. Opin. Cell Biol. *17*, 47–54.

Ammer, A.G., and Weed, S.A. (2008). Cortactin branches out: Roles in regulating protrusive actin dynamics. Cell Motil. Cytoskeleton *65*, 687–707.

Basu, R., and Chang, F. (2007). Shaping the actin cytoskeleton using microtubule tips. Curr. Opin. Cell Biol. *19*, 88–94.

Bougneres, L., Girardin, S.E., Weed, S.A., Karginov, A.V., Olivo-Marin, J.C., Parsons, J.T., Sansonetti, P.J., and Van Nhieu, G.T. (2004). Cortactin and Crk cooperate to trigger actin polymerization during Shigella invasion of epithelial cells. J. Cell Biol. *166*, 225–235.

Chicurel, M.E., and Harris, K.M. (1992). Three-dimensional analysis of the structure and composition of CA3 branched dendritic spines and their synaptic relationships with mossy fiber boutons in the rat hippocampus. J. Comp. Neurol. *325*, 169–182.

Chin, L.S., Nugent, R.D., Raynor, M.C., Vavalle, J.P., and Li, L. (2000). SNIP, a novel SNAP-25-interacting protein implicated in regulated exocytosis. J. Biol. Chem. *275*, 1191–1200.

Dent, E.W., and Gertler, F.B. (2003). Cytoskeletal dynamics and transport in growth cone motility and axon guidance. Neuron *40*, 209–227.

Di Stefano, P., Cabodi, S., Boeri Erba, E., Margaria, V., Bergatto, E., Giuffrida, M.G., Silengo, L., Tarone, G., Turco, E., and Defilippi, P. (2004). P130Cas-associated protein (p140Cap) as a new tyrosine-phosphorylated protein involved in cell spreading. Mol. Biol. Cell *15*, 787–800.

Di Stefano, P., Damiano, L., Cabodi, S., Aramu, S., Tordella, L., Praduroux, A., Piva, R., Cavallo, F., Forni, G., Silengo, L., et al. (2007). p140Cap protein suppresses tumour cell properties, regulating Csk and Src kinase activity. EMBO J. *26*, 2843–2855.

Dosemeci, A., Makusky, A.J., Jankowska-Stephens, E., Yang, X., Slotta, D.J., and Markey, S.P. (2007). Composition of the synaptic PSD-95 complex. Mol. Cell. Proteomics *6*, 1749–1760.

Ethell, I.M., and Pasquale, E.B. (2005). Molecular mechanisms of dendritic spine development and remodeling. Prog. Neurobiol. *75*, 161–205.

Frame, M.C., Fincham, V.J., Carragher, N.O., and Wyke, J.A. (2002). v-Src's hold over actin and cell adhesions. Nat. Rev. Mol. Cell Biol. *3*, 233–245.

Gu, C., Zhou, W., Puthenveedu, M.A., Xu, M., Jan, Y.N., and Jan, L.Y. (2006). The microtubule plus-end tracking protein EB1 is required for Kv1 voltage-gated K+ channel axonal targeting. Neuron *52*, 803–816.

Harris, K.M., and Kater, S.B. (1994). Dendritic spines: cellular specializations imparting both stability and flexibility to synaptic function. Annu. Rev. Neurosci. *17*, 341–371.

He, Y., Yu, W., and Baas, P.W. (2002). Microtubule reconfiguration during axonal retraction induced by nitric oxide. J. Neurosci. *22*, 5982–5991.

Hering, H., and Sheng, M. (2001). Dendritic spines: structure, dynamics and regulation. Nat. Rev. Neurosci. *2*, 880–888.

Hering, H., and Sheng, M. (2003). Activity-dependent redistribution and essential role of cortactin in dendritic spine morphogenesis. J. Neurosci. *23*, 11759–11769.

Hirokawa, N., and Takemura, R. (2005). Molecular motors and mechanisms of directional transport in neurons. Nat. Rev. Neurosci. *6*, 201–214.

Hoogenraad, C.C., Milstein, A.D., Ethell, I.M., Henkemeyer, M., and Sheng, M. (2005). GRIP1 controls dendrite morphogenesis by regulating EphB receptor trafficking. Nat. Neurosci. *8*, 906–915.

Jaworski, J., Hoogenraad, C.C., and Akhmanova, A. (2008). Microtubule plus-end tracking proteins in differentiated mammalian cells. Int. J. Biochem. Cell Biol. *40*, 619–637.

Kaech, S., Parmar, H., Roelandse, M., Bornmann, C., and Matus, A. (2001). Cytoskeletal microdifferentiation: a mechanism for organizing morphological plasticity in dendrites. Proc. Natl. Acad. Sci. USA *98*, 7086–7092.

Kasai, H., Matsuzaki, M., Noguchi, J., Yasumatsu, N., and Nakahara, H. (2003). Structure-stability-function relationships of dendritic spines. Trends Neurosci. *26*, 360–368.

Kaufmann, W.E., and Moser, H.W. (2000). Dendritic anomalies in disorders associated with mental retardation. Cereb. Cortex *10*, 981–991.

Kennedy, M.J., and Ehlers, M.D. (2006). Organelles and trafficking machinery for postsynaptic plasticity. Annu. Rev. Neurosci. *29*, 325–362.

Kennedy, M.B., Beale, H.C., Carlisle, H.J., and Washburn, L.R. (2005). Integration of biochemical signalling in spines. Nat. Rev. Neurosci. *6*, 423–434.

Kneussel, M. (2005). Postsynaptic scaffold proteins at non-synaptic sites. The role of postsynaptic scaffold proteins in motor-protein-receptor complexes. EMBO Rep. *6*, 22–27.

Komarova, Y., Lansbergen, G., Galjart, N., Grosveld, F., Borisy, G.G., and Akhmanova, A. (2005). EB1 and EB3 control CLIP dissociation from the ends of growing microtubules. Mol. Biol. Cell *16*, 5334–5345.

Lamprecht, R., and LeDoux, J. (2004). Structural plasticity and memory. Nat. Rev. Neurosci. *5*, 45–54.

Landis, D.M., and Reese, T.S. (1983). Cytoplasmic organization in cerebellar dendritic spines. J. Cell Biol. *97*, 1169–1178.

Lansbergen, G., and Akhmanova, A. (2006). Microtubule plus end: a hub of cellular activities. Traffic *7*, 499–507.

Lynch, D.K., Winata, S.C., Lyons, R.J., Hughes, W.E., Lehrbach, G.M., Wasinger, V., Corthals, G., Cordwell, S., and Daly, R.J. (2003). A Cortactin-CD2-associated protein (CD2AP) complex provides a novel link between epidermal growth factor receptor endocytosis and the actin cytoskeleton. J. Biol. Chem. *278*, 21805–21813.

Martinez-Quiles, N., Ho, H.Y., Kirschner, M.W., Ramesh, N., and Geha, R.S. (2004). Erk/Src phosphorylation of cortactin acts as a switch on-switch off mechanism that controls its ability to activate N-WASP. Mol. Cell. Biol. *24*, 5269–5280.

Matus, A. (2000). Actin-based plasticity in dendritic spines. Science *290*, 754–758.

Mimori-Kiyosue, Y., Shiina, N., and Tsukita, S. (2000). Adenomatous polyposis coli (APC) protein moves along microtubules and concentrates at their growing ends in epithelial cells. J. Cell Biol. *148*, 505–518.

Morita, A., Yamashita, N., Sasaki, Y., Uchida, Y., Nakajima, O., Nakamura, F., Yagi, T., Taniguchi, M., Usui, H., Katoh-Semba, R., et al. (2006). Regulation of dendritic branching and spine maturation by semaphorin3A-Fyn signaling. J. Neurosci. *26*, 2971–2980.

Morrison, E.E., Moncur, P.M., and Askham, J.M. (2002). EB1 identifies sites of microtubule polymerisation during neurite development. Brain Res. Mol. Brain Res. *98*, 145–152.

Naisbitt, S., Kim, E., Tu, J.C., Xiao, B., Sala, C., Valtschanoff, J., Weinberg, R.J., Worley, P.F., and Sheng, M. (1999). Shank, a novel family of postsynaptic density proteins that binds to the NMDA receptor/PSD-95/GKAP complex and cortactin. Neuron *23*, 569–582.

Nakagawa, H., Koyama, K., Murata, Y., Morito, M., Akiyama, T., and Nakamura, Y. (2000). EB3, a novel member of the EB1 family preferentially expressed in the central nervous system, binds to a CNS-specific APC homologue. Oncogene *19*, 210–216.

Newey, S.E., Velamoor, V., Govek, E.E., and Van Aelst, L. (2005). Rho GTPases, dendritic structure, and mental retardation. J. Neurobiol. *64*, 58–74.

Okamoto, K., Nagai, T., Miyawaki, A., and Hayashi, Y. (2004). Rapid and persistent modulation of actin dynamics regulates postsynaptic reorganization underlying bidirectional plasticity. Nat. Neurosci. *7*, 1104–1112.

Peng, J., Kim, M.J., Cheng, D., Duong, D.M., Gygi, S.P., and Sheng, M. (2004). Semiquantitative proteomic analysis of rat forebrain postsynaptic density fractions by mass spectrometry. J. Biol. Chem. *279*, 21003–21011.

Rodriguez, O.C., Schaefer, A.W., Mandato, C.A., Forscher, P., Bement, W.M., and Waterman-Storer, C.M. (2003). Conserved microtubule-actin interactions in cell movement and morphogenesis. Nat. Cell Biol. *5*, 599–609.

Shaw, R.M., Fay, A.J., Puthenveedu, M.A., von Zastrow, M., Jan, Y.N., and Jan, L.Y. (2007). Microtubule plus-end-tracking proteins target gap junctions directly from the cell interior to adherens junctions. Cell *128*, 547–560.

Sheng, M., and Hoogenraad, C.C. (2007). The postsynaptic architecture of excitatory synapses: a more quantitative view. Annu. Rev. Biochem. *76*, 823–847.

Siegrist, S.E., and Doe, C.Q. (2007). Microtubule-induced cortical cell polarity. Genes Dev. *21*, 483–496.

Stehbens, S.J., Paterson, A.D., Crampton, M.S., Shewan, A.M., Ferguson, C., Akhmanova, A., Parton, R.G., and Yap, A.S. (2006). Dynamic microtubules regulate the local concentration of E-cadherin at cell-cell contacts. J. Cell Sci. *119*, 1801–1811.

Stepanova, T., Slemmer, J., Hoogenraad, C.C., Lansbergen, G., Dortland, B., De Zeeuw, C.I., Grosveld, F., van Cappellen, G., Akhmanova, A., and Galjart, N. (2003). Visualization of microtubule growth in cultured neurons via the use of EB3-GFP (end-binding protein 3-green fluorescent protein). J. Neurosci. *23*, 2655–2664.

Suter, D.M., Schaefer, A.W., and Forscher, P. (2004). Microtubule dynamics are necessary for SRC family kinase-dependent growth cone steering. Curr. Biol. *14*, 1194–1199.

Tada, T., and Sheng, M. (2006). Molecular mechanisms of dendritic spine morphogenesis. Curr. Opin. Neurobiol. *16*, 95–101.

Trinidad, J.C., Specht, C.G., Thalhammer, A., Schoepfer, R., and Burlingame, A.L. (2006). Comprehensive identification of phosphorylation sites in postsynaptic density preparations. Mol. Cell. Proteomics *5*, 914–922.

van Rossum, D., and Hanisch, U.K. (1999). Cytoskeletal dynamics in dendritic spines: direct modulation by glutamate receptors? Trends Neurosci. *22*, 290–295.

Vasquez, R.J., Howell, B., Yvon, A.M., Wadsworth, P., and Cassimeris, L. (1997). Nanomolar concentrations of nocodazole alter microtubule dynamic instability in vivo and in vitro. Mol. Biol. Cell *8*, 973–985.

Weaver, A.M., Young, M.E., Lee, W.L., and Cooper, J.A. (2003). Integration of signals to the Arp2/3 complex. Curr. Opin. Cell Biol. *15*, 23–30.

Webb, D.J., Zhang, H., Majumdar, D., and Horwitz, A.F. (2007). alpha5 integrin signaling regulates the formation of spines and synapses in hippocampal neurons. J. Biol. Chem. *282*, 6929–6935.

Westrum, L.E., Jones, D.H., Gray, E.G., and Barron, J. (1980). Microtubules, dendritic spines and spine appratuses. Cell Tissue Res. *208*, 171–181.

Wu, H., and Parsons, J.T. (1993). Cortactin, an 80/85-kilodalton pp60src substrate, is a filamentous actin-binding protein enriched in the cell cortex. J. Cell Biol. *120*, 1417–1426.

Yuste, R., and Bonhoeffer, T. (2001). Morphological changes in dendritic spines associated with long-term synaptic plasticity. Annu. Rev. Neurosci. *24*, 1071–1089.